Int J Thermophys (2016) 37:82
DOI 10.1007/s10765-016-2090-9

ICPPP 18

Contact Pattern Analysis: Simulation of a Laser-Assisted Thermographic Approach

H. Prekel[1] · G. Stroebel[1] · R. Lipinski[1] · G. Goch[1,2]

Received: 4 September 2015 / Accepted: 11 June 2016 / Published online: 24 June 2016
© Springer Science+Business Media New York 2016

Abstract The contact pattern, defined as the area where gear teeth come into contact during their meshing, is a crucial quality feature of gears. If the size and location of the contact pattern are wrong, the gear meshing properties can be significantly affected (e.g., lifetime, noise). Despite several disadvantages, the so-called "paste method" is established as a method to analyse contact patterns. Here, a new measuring approach is examined using the Finite Elements Method (FEM). It is based on the heating-up of one tooth flank with a powerful laser, a subsequent partial transfer of the heat to a meshing tooth of the second gear wheel and finally capturing the heat distribution on that flank as an infrared image shortly afterwards. The thermal image should correspond to the contact pattern of that individual combination of teeth. A numerical analysis shows that at medium- and large-sized gears the achievable temperature increase will be high enough to be detected with modern infrared cameras.

Keywords Contact pattern analysis · Finite elements method · Gears · Heat transfer

1 Introduction

Gears and gearwheels, which exist in many forms and sizes, belong to the key components of propulsion technology. The production of gearwheels and the measurement of

This article is part of the selected papers presented at the 18th International Conference on Photoacoustic and Photothermal Phenomena.

✉ H. Prekel
pre@bimaq.de

1 University of Bremen/ BIMAQ, Bremen, Germany

2 Department of Mechanical Engineering and Engineering Science, University of North Carolina at Charlotte, Charlotte, USA

their geometries often prove to be very challenging [1,2]. The interaction of gearwheels depends on the accuracy of their geometries, their precise alignment in housings and possible deformations of gear housings under load. The combination of form deviations, fitting errors and deformations causes that the contact pattern is difficult to predict. The contact patterns should be located in the middle of tooth flanks where the mechanical strength is at maximum. Incorrect contact patterns can lead to excessive friction and high pressure values at the edges of gear teeth, causing increased wear, decreased efficiency and sometimes fractures of teeth. The usual method for the detection of contact patterns is the so-called "paste method" [3]: the gearwheel teeth are coated with a special paint, which is rubbed away during meshing. Areas without paint then correspond to the sought contact pattern. Disadvantages are the cumbersome documentation of results (photos, transfer pictures with adhesive strips) and the required time, lasting from some hours up to two days for a gearwheel pair. Other disadvantages are the low degree of automation and the fact that after multiple meshing the result is an average contact pattern, which develops after many contacts of a certain tooth flank with many or all flanks of the second involved gearwheel. As an alternative, a passive thermographic approach to analyse contact patterns was examined in [4–6]. However, the former state of development disqualified infrared cameras for this application. Furthermore, the passive thermography must be considered as critical, because it is based on the detection of frictional heat, which gear manufacturers try to minimize in order to improve the efficiency of gears. Additionally, during the meshing of gear teeth, the heat production is not constant or even zero, which may cause errors in measurement and interpretation. This paper proposes a new, laser-assisted approach, which had been modelled by FEM analysis in order to find out which temperature increase can be expected in practice. It consists of the heating-up of a tooth flank by laser radiation, a subsequent heat transfer to the meshing tooth flank of a second gear wheel and finally the detection of the temperature distribution on that flank by an infrared camera [7].

2 Software Strategy and Simplified Geometry

Elaborating a model for the measurement process required to develop a special software strategy and a simplified gear tooth geometry due to the limited capabilities of the applied FEM software. An important limitation was implied by the fact that the software did not support the meshing movement of gear teeth sufficiently. Hence, a substitute tooth geometry in the form of a trapezoidal cylinder was chosen (Fig. 1a, b), which has only flat surfaces and is similar to real gear teeth with respect to heat diffusion. The smaller part of each cylinder represents a tooth, whereas the larger part corresponds to the gear's base body and acts as a heat sink. The heat transfer between the teeth during meshing can be realized by assuming that both involved tooth flanks touch each other with almost their complete surfaces (here: about 85 %) and allowing a heat flux only at a small partial area which is moving along the tooth flanks (Fig. 1c). The constant mechanical contact of both cylinders, however, complicates the formulation of boundary conditions during the laser heating: expressing the absorption of radiation energy into tooth flank A resulted in a temperature increase in both cylin-

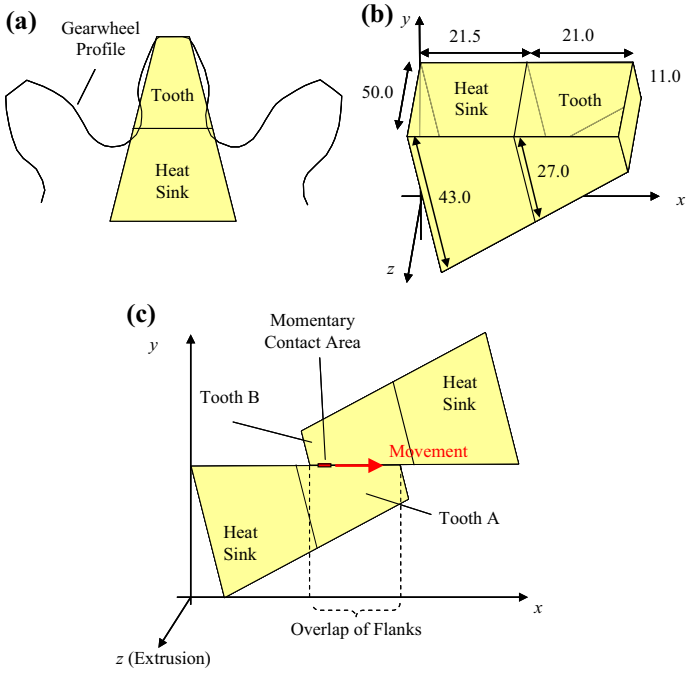

Fig. 1 Simplified tooth geometry: (a) cross section, (b) selected dimensions, in mm, (c) overlapping tooth flanks with moving momentary contact area

ders, which is unrealistic. This effect was avoided by declaring tooth B as an "external object", by which a constant temperature of zero °C, arbitrarily defined as ambient temperature, is allocated to it.

Then, the boundary condition will only affect tooth A. Initially, the implanted energy will propagate only within tooth A. All surfaces in contact with air are assumed to be thermally isolated. The temperature distribution calculated for the moment shortly before the contact is stored and then recalled by a second FEM script, which calculates the further heat diffusion, working with the same geometries, but different boundary conditions:

tooth B now becomes an "internal object", and the former boundary condition is replaced by a contact-resistance boundary condition, which allows a heat flux Θ at the interface, depending on the temperature difference ΔT and the thermal contact resistance R:

$$\Theta = \Delta T / R \quad \text{in W·m}^{-2} \tag{1}$$

The thermal contact resistance is set to a low value at regions where the contact takes place and to a very high value elsewhere. During and after the contact, heat will propagate within both teeth.

The complete simulated measurement process can be divided into four phases:
Phase I: heating-up of tooth flank A by laser radiation.
Phase II: heat propagation within tooth A.
Phase III: contact of both flanks with heat transfer from tooth A to tooth B and heat propagation in both teeth.
Phase IV: heat propagation within both teeth after the contact until the infrared camera captures an image.

3 Simulation Parameters

The selected simulation parameters correspond to a medium-sized cylindrical gear wheel (diameter $\approx$ 530 mm, 41 teeth). For simplicity, a gear with identical gear wheels is considered. The thermal conductivity was κ = 45 $Wm^{-1}{\cdot}K^{-1}$ and the thermal diffusivity $\alpha = 1.18 \times 10^{-5}$ $m^2{\cdot}s^{-1}$. The meshing parameters are illustrated in Fig. 2. The momentary contact area xb is moving with the speed $v = (xe - xs)/tc$ (tc = contact time of both flanks) along the overlapping surfaces to the right, allowing a local heat flux Θ corresponding to Eq. 1. After meshing, R is assigned a very high value, thermally isolating both teeth completely from each other. The z-extension of the momentary contact area was defined as zb = 20 mm, and therefore smaller than the tooth width (50 mm). The absorbed laser power density, applied homogeneously to the whole flank A, was set to 10^6 $W{\cdot}m^{-2}$, an amount that can be achieved on the simulated flanks with 3 kW of laser power at about 30% absorption rate. On the basis of an exemplary gear wheel design, the following angles were defined for the four

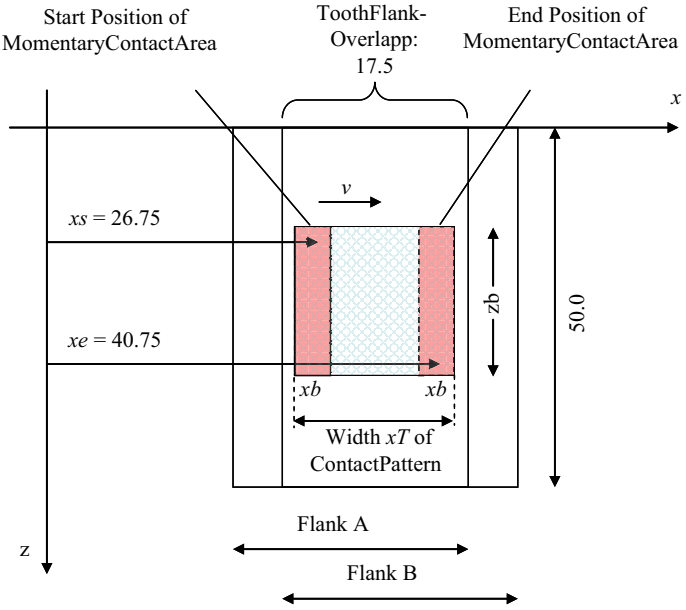

Fig. 2 Overlapping tooth flanks with contact pattern and start/end-positions of the momentary contact area. (All parameters in mm)

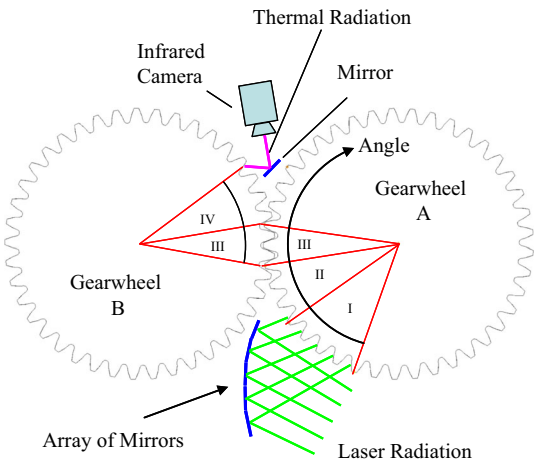

Fig. 3 Illustration of angles for the four phases of the detection process

phases of the measurement process (Fig. 3): $\varphi_{II} = 28°$, $\varphi_{III} = 14°$, $\varphi_{IV} = 28°$. The angle φ_I depends on the available space for laser excitation within the gear. It was set to 56° for this study. Assuming a time of rotation of $t_u = 25.7$ s and a constant angular velocity for the gear wheels, the time periods t_i for each of the four phases results from the angles φ_i by $t_i = \varphi_i \cdot t_u / 360°$, giving $t_I = 4$ s, $t_{II} = 2$ s, $t_{III} = 1$ s and $t_{IV} = 2$ s. The ratio of these time periods will be the same for other rotation times.

4 Results

4.1 Influence of the Thermal Contact Resistance

The thermal contact resistance R respectively the heat transfer coefficient $F = 1/R$ of an interface is difficult to quantify, because it depends on the contacting materials, the pressure between the involved objects, their surface roughness and maybe lubricants like oil [8–10]. As precise values are unknown, FEM calculations were performed within a wide range of the heat transfer coefficient, namely F = 1000, 3500 and 10 000 $W \cdot K^{-1} \cdot m^{-2}$. The other parameters were set to $xb = 1.75$ mm, $zb = 20$ mm, t_u = 5.14 s and $v = 70$ mm/s (Fig. 2). Figure 4 illustrates the simulated temperature increase at the end of phase IV (the moment of infrared detection) of tooth B at z = 25 mm from the top to the bottom of the tooth and very close beneath the surface (the surface temperature itself could not be extracted from the software). The temperatures roughly scale with the heat transfer coefficient, enabeling to calculate temperature curves for other values of F just by interpolation.

4.2 Influence of the Time of Rotation

For the next simulations, the heat transfer coefficient had been kept constant at F = 3500 $W \cdot K^{-1} \cdot m^{-2}$ and the time of rotation was varied between $t_u = 2.57$ s and t_u =

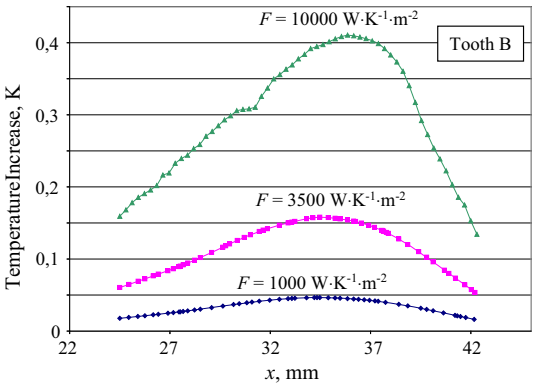

Fig. 4 Temperature curves on the flank of tooth B at the end of phase IV, calculated for different heat transfer coefficients F of the interface

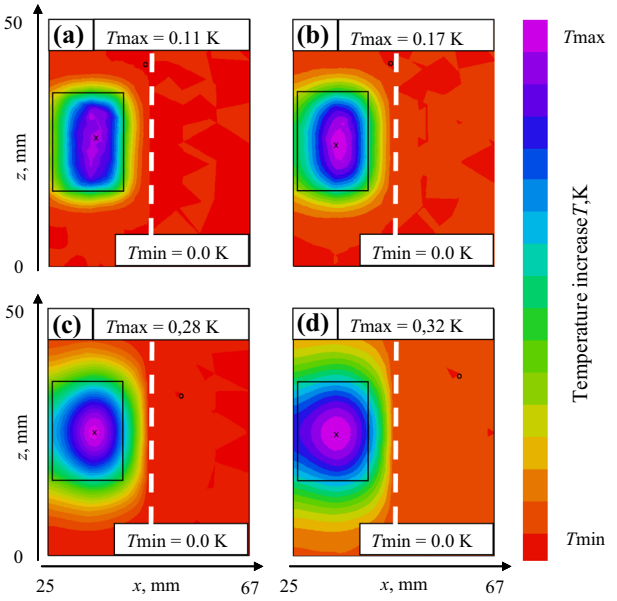

Fig. 5 Temperature distribution on the flank of tooth B at the end of phase IV, calculated for different times of rotation t_u : (a) 2.57 s, (b) 5.14 s, (c) 12.85 s, (d) 25.7 s

25.7 s. Figure 5 shows the distribution of temperature increase on the flank of tooth B. The left half of each image (up to the dashed line) corresponds to the tooth flank, the right half to the heat sink, who's temperature will not be detectable by radiometry in practice. The rectangle in each subimage indicates the contact pattern, which is xT = 15.65 mm wide. The width of the momentary contact area again was set to xb = 1.75 mm. In Fig. 5a the time span t_{IV} is 0.2 s. Within this time, the heat transferred from tooth A to tooth B cannot propagate significantly; hence, the temperature distribution is a good representation of the contact pattern. The temperature increase of 30 mK to 110 mK within the contact pattern can be detected with modern infrared cameras, especially if a thin film of oil on the tooth flanks improves their infrared emission.

Increased times of rotation will provide more time for absorbing radiation energy and more time for the heat transfer from tooth A to tooth B, causing a higher temperature increase on flank B (Fig. 5b to d). However, the heat has more time to propagate within both teeth, and the temperature distribution, especially in Figure 8d, is only a very blurred image of the contact pattern.

4.3 Influence of the Width of the Momentary Contact Area

Finally, the influence of the width *xb* of the momentary contact area was examined. t_u was set to 5.14 s and F to 3500 $\mathrm{W{\cdot}K^{-1}{\cdot}m^{-2}}$. The parameter *xb* was varied from 0.4 mm to 3.5 mm: the calculated maximum temperature increases on tooth flank B at the end of phase IV ranged from 40 mK to 320 mK (not shown). At $xb = 0.4$ mm, the temperature increase at the margins of the contact pattern will be about 10 mK, which is below the detection limit of modern infrared cameras ($\approx$15 mK). This means that *xb* should be significantly above 0.4 mm. According to the laws of contact mechanics, *xb* increases with the radius of tooth flank curvature and with torque. Consequently, large values for *xb* (e.g., $\mathrm{xb} \geq 1$ mm) can be expected especially in large-dimensioned gears like those in wind power plants. In smaller gears like those of automobiles, *xb* is probably too small to allow a sufficient heat transfer from tooth A to tooth B to be detected by thermography.

5 Conclusion and Outlook

In this work, a laser-assisted approach for the contact pattern analysis was examined. It showed that in large-dimensioned gear wheels, a detectable heat transfer from one tooth to another tooth can be expected, promising high chances of success for the new method and justifying subsequent experimental work. In smaller gears, the measurement conditions (high rotational speed, lower torque values) are less promising. In addition to the experimental verification of the simulation results, the blurring effect of infrared images will be one of the subjects for future research work. First efforts to reconstruct the contact patterns from blurred infrared images by software algorithms are encouraging. In some cases, the test conditions could possibly be improved by varying the angular velocity of the gearwheels: decreasing the time for phases II and IV will increase the temperatures on tooth flank B and reduce the blurring by heat diffusion. Further research work must also show the influence of oil films (thickness, radiation properties) on the gear teeth as well as frictional heat which might superimpose the laser-generated heat.

Acknowledgments The authors would like to thank the German Research Foundation (DFG) for funding the research project, Reference Number GO 554/32-1.

References

1. G. Goch, in VDI-Berichte 1880, pp 1–23 (2005)
2. A. Günther, Doctor-Thesis, Bremen (2008)

3. J. Goebbelet, Doctor-Thesis, Aachen (1980)
4. H. Wüstner, Deutsches Patentamt. Offenlegungsschrift DE 3136613 A1 (1983)
5. J. Grabscheid, Doctor-Thesis, Stuttgart (1989)
6. G. Neumann, Doctor-Thesis, Stuttgart (1995)
7. H. Prekel, H. Gafsi, G. Goch. Deutsches Patentamt, Offenlegungsschrift DE102012003814A1 (2013)
8. C. Fieberg, R. Kneer, Int. J. Heat Transfer **51**, 1017–1023 (2008)
9. M.R. Sridhar, M.M. Yovanovich, Int. J. Heat Transfer **39**(4), 831–839 (1995)
10. R. Dou, T. Ge, X. Liu, Z. Wen, Int. J. Heat Transfer **94**, 156–163 (2016)